

Supplementary Information

Interfacial Nanobubbles' Growth at the Initial Stage of Electrocatalytic Hydrogen Evolution

Jinwen Yu^a, Kadi Hu^b, Zhengyi Zhang^a, Liang Luo^{a*}, Yiwei Liu^a, Daojin Zhou^a, Fengmei Wang^a,

Yun Kuang^a, Haijun Xu^a, Hui Li^{b*}, Haohong Duan^c, and Xiaoming Sun^{a*}

*Correspondence and requests for materials should be addressed to Liang Luo (luoliang@mail.buct.edu.cn), Hui Li (hli@mail.buct.edu.cn) or Xiaoming Sun (sunxm@mail.buct.edu.cn).

Contents

Supplementary Tables.....	2
Supplementary Figures.....	3

Supplementary Tables

	H-H	W-W	E-E	A-A	H-E	H-A	W-E	W-A
\mathcal{E} (kcal/mol)	0.022	0.155	5.29	5.29	0.334	0.115	0.453	0.906
σ (Å)	2.683	3.169	2.951	2.951	2.817	2.817	2.937	3.292

Table S1. Interaction parameters between atoms. H represents the atom of a hydrogen molecule; W represents the O atom of a water molecule while the interaction parameters of the H atom in the water molecule are both 0; E the atom of electrode; A the atoms of the hydrophilic layer surrounding the electrode.

Supplementary Figures

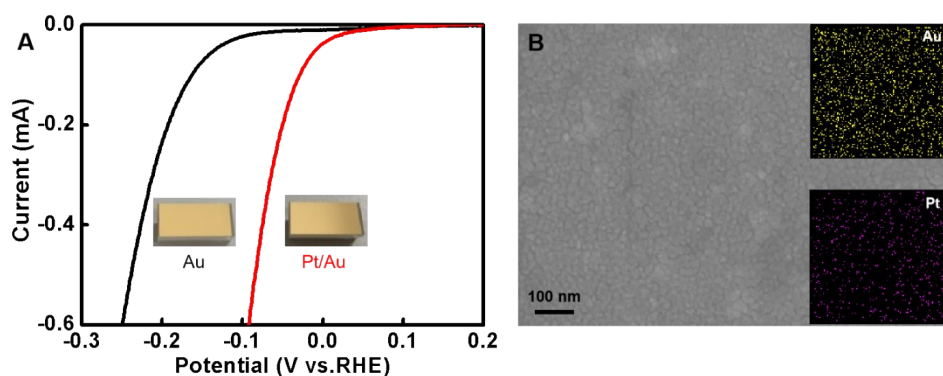


Fig. S1 (A) Linear sweep voltammetry curve of hydrogen evolution reaction (HER) before and after platinum plating and (B) is the corresponding element distribution after platinum plating.

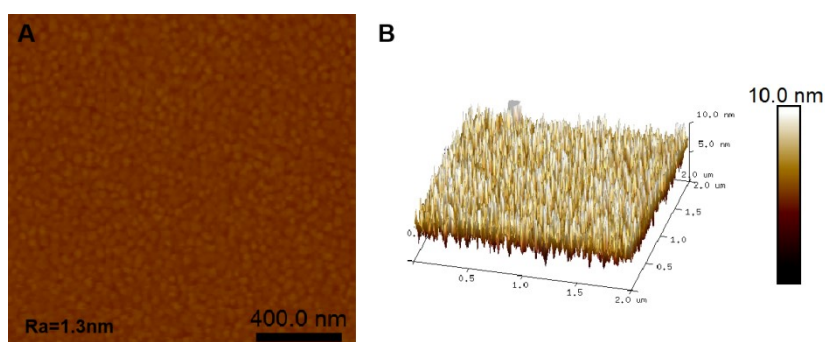


Fig. S2 (A) AFM and (B) 3D view images of Au electrode after platinum plating.

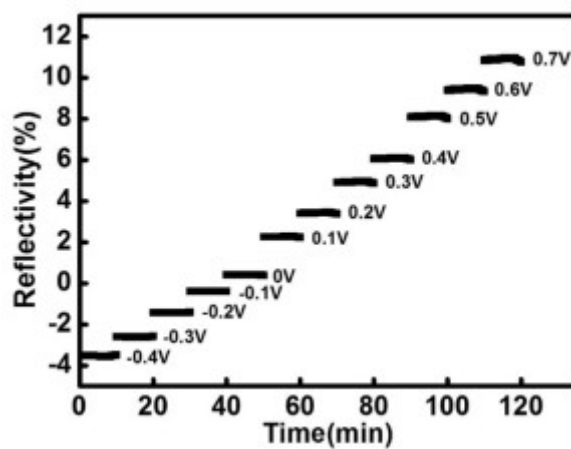


Fig. S3 Variation of balanced reflectivity baselines of SPR curves at potentials from -0.4 V to 0.7 V.

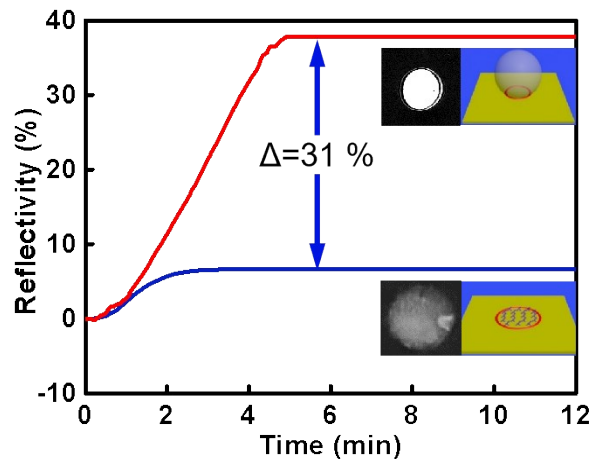


Fig. S4 Time-dependent reflectivity curves of single bubble evolution (36%) and reference DNA molecules binding (7%), inset: differential images and the side-view schemes of the contact area of single bubble and the binding area of DNA molecules.

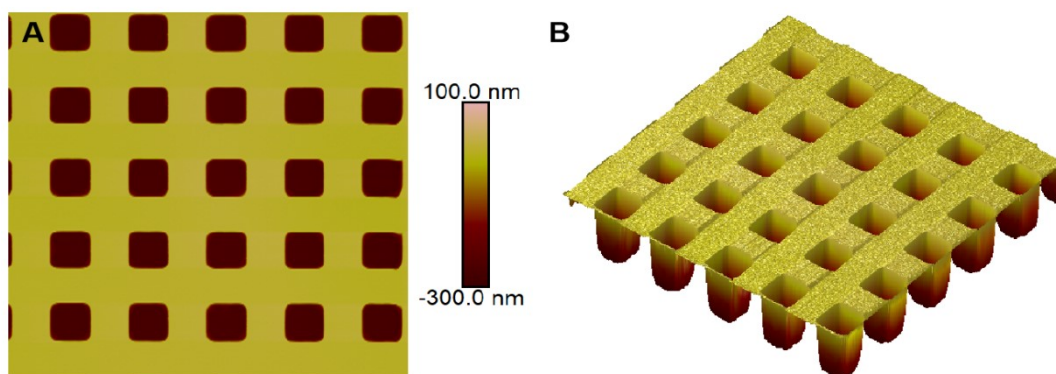


Fig. S5 Tip correction of AFM.

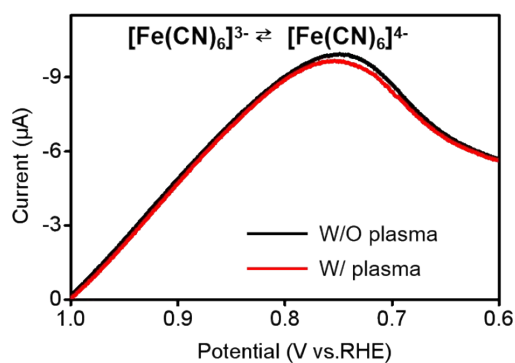


Fig. S6 The LSV oxidation curves of $[\text{Fe}(\text{CN})_6]^{3-} \leftrightarrow [\text{Fe}(\text{CN})_6]^{4-}$ recorded on electrodes with (the red line) and without (the black line) oxygen plasma treatment.

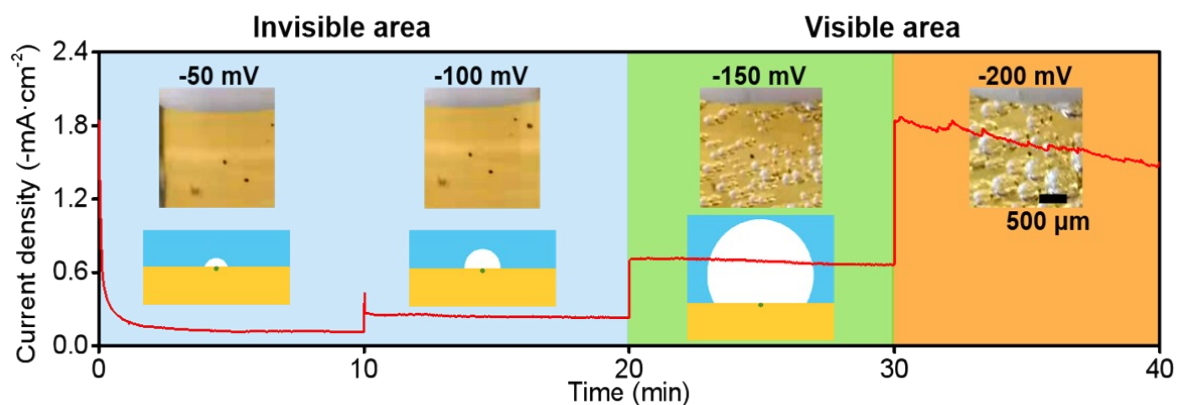


Fig. S7 Overpotential-dependent current steps before ($V \leq 100\text{mV}$) and after ($V \geq 150\text{mV}$) formation of macroscopic bubbles, and the corresponding bubbles' images on electrodes.

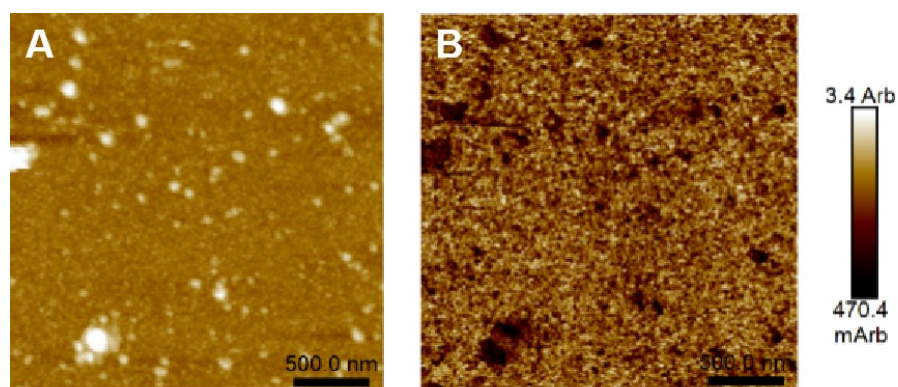


Fig. S8 (A) AFM image of nanobubbles and (B) DMT Modulus (contact force) test.

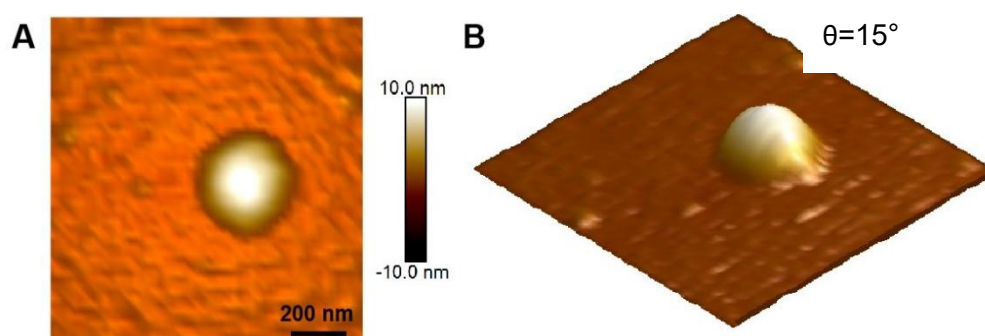


Fig. S9 AFM and 3D view images of nanobubble pancake appeared on the electrode surface after 10 minutes of HER.

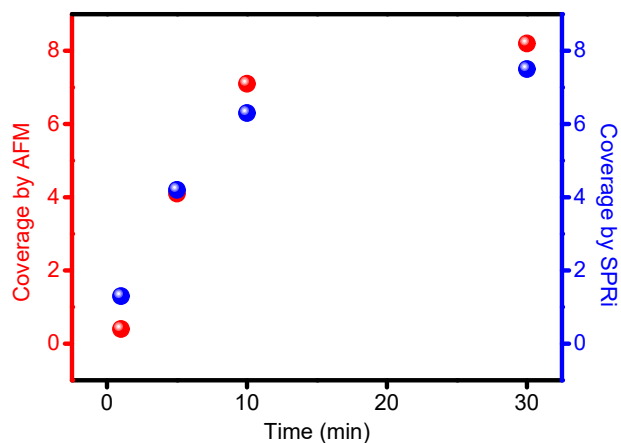


Fig. S10 Comparison of time-dependent variations of nanobubble coverage by AFM and SPR.

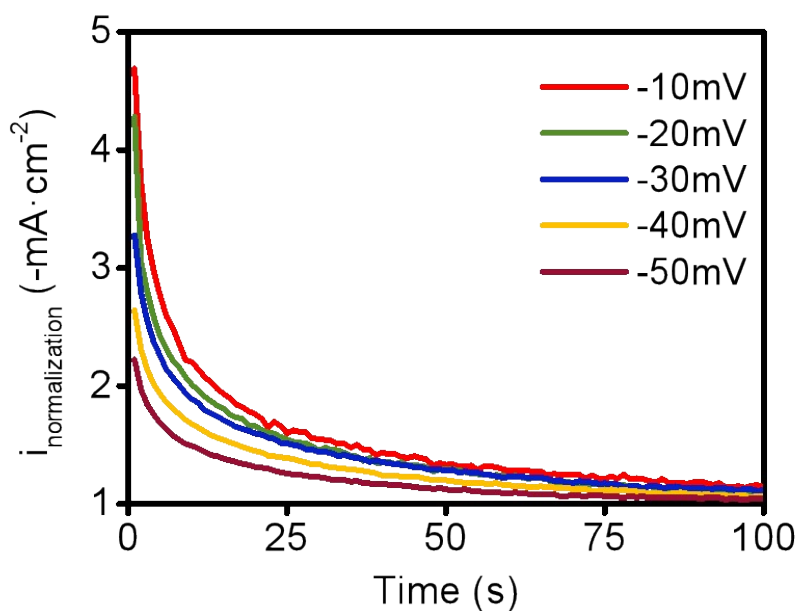


Fig. S11 Normalized time-dependent current variations at different overpotentials.

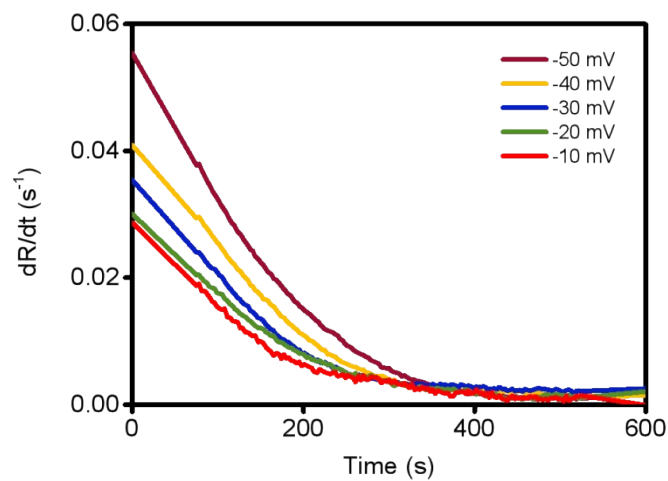


Fig. S12 Differential curves of reflectivity at different overpotentials.

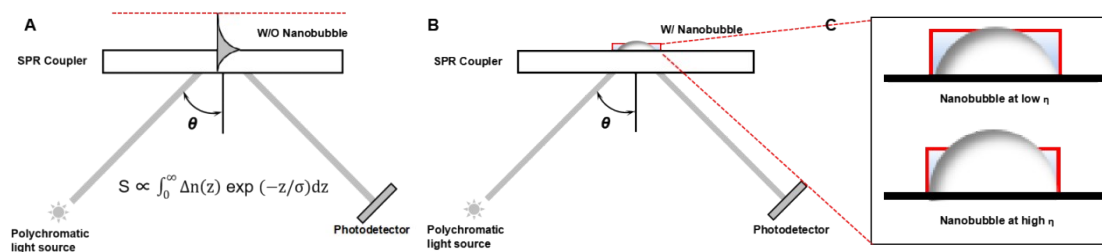


Fig. S13 Longitudinal variation of the evanescent wave on the electrode surface: A) without nanobubbles; B) with nanobubbles; C) nanobubbles with different geometries.

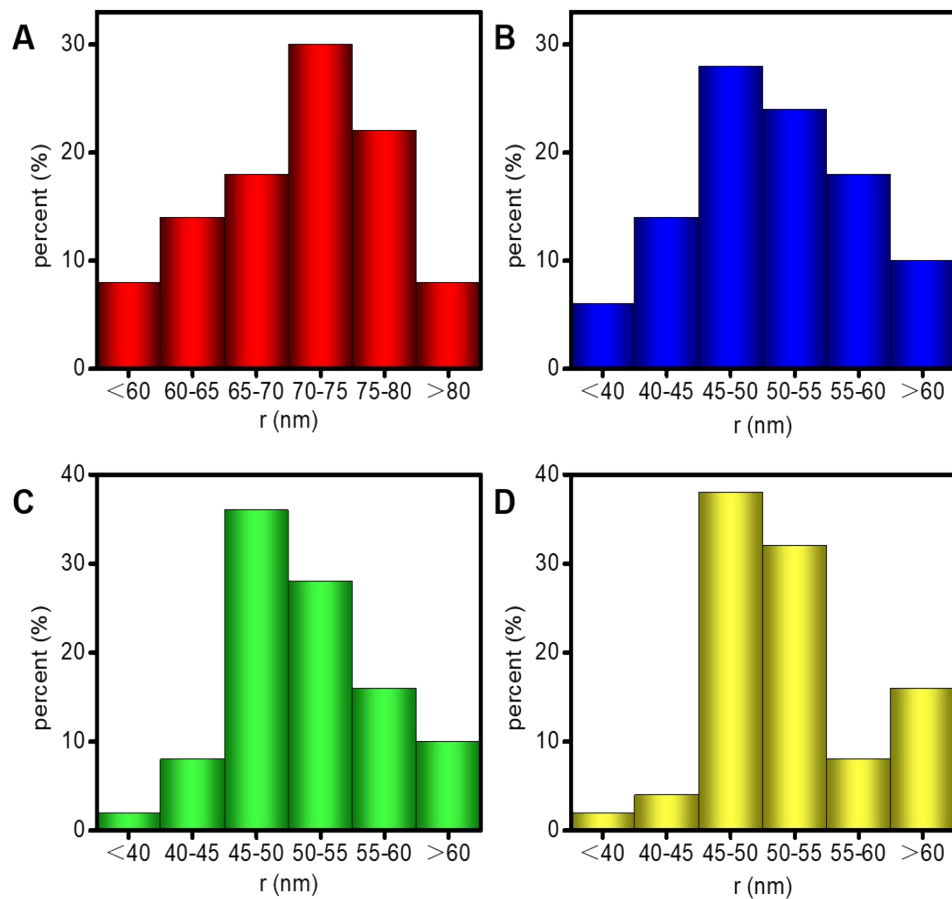


Fig. S14 Size distribution of nanobubbles at (A) 1 min, (B) 5 min, (C) 10 min and (D) 30 min.

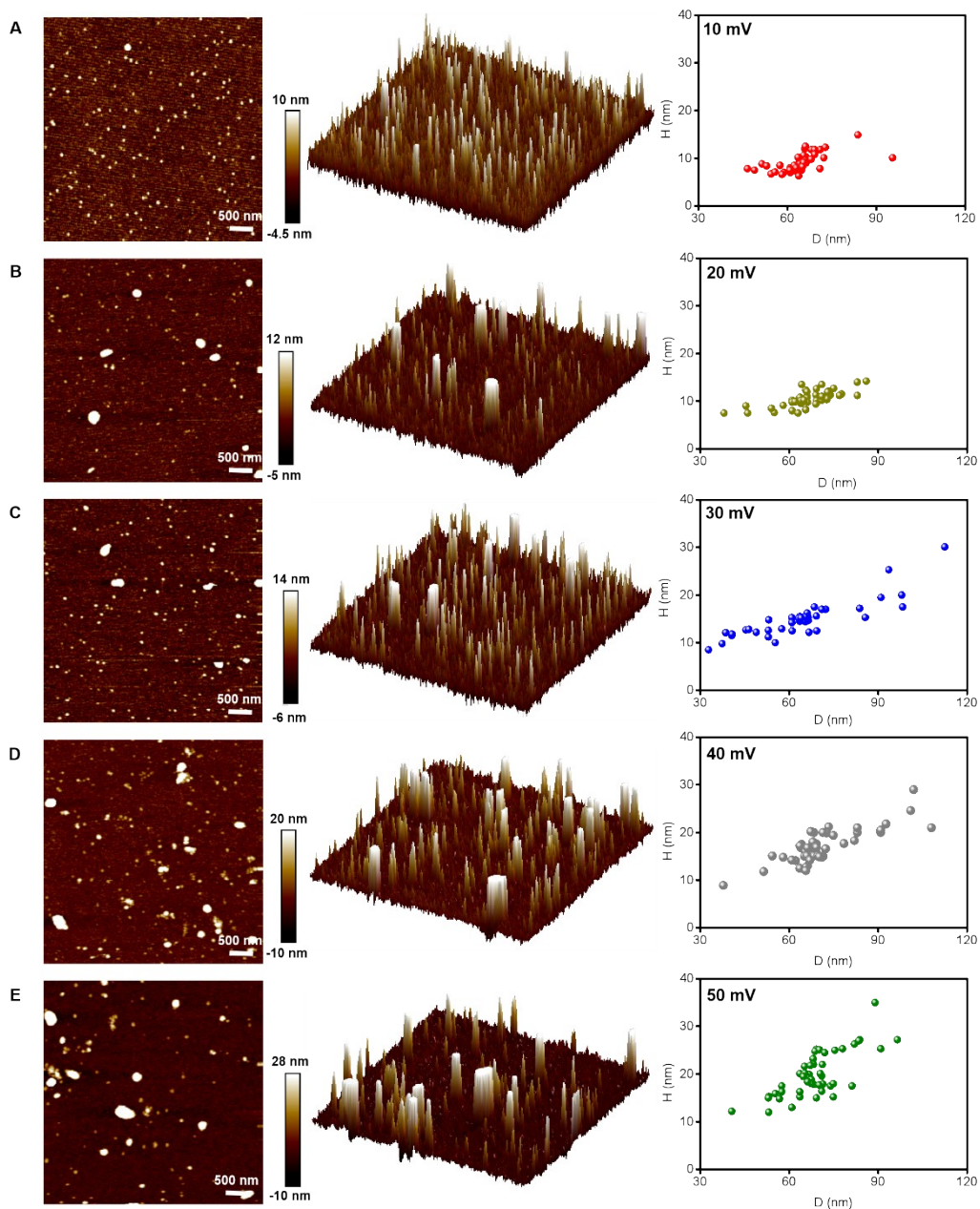


Fig. S15 Size distribution of nanobubbles under different overpotentials.

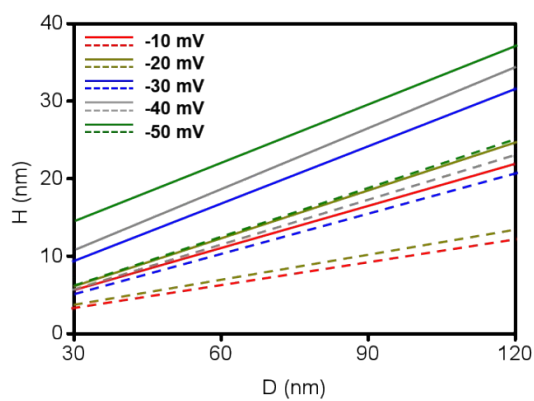


Fig. S16 Distribution range of nanobubbles at different overpotentials

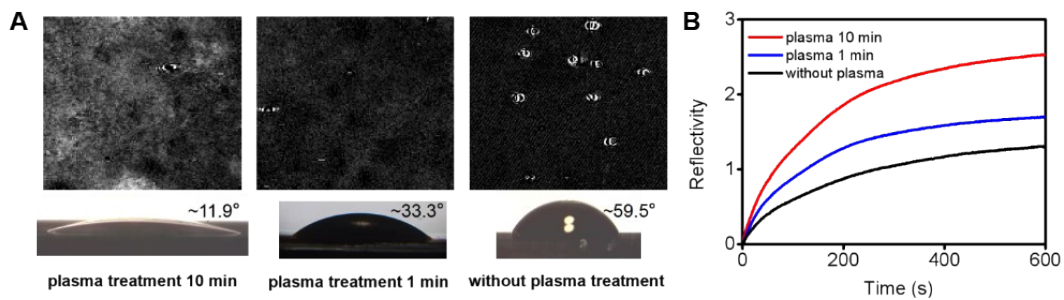


Fig. S17 Under 50 mV overpotential, the nanobubbles generated(A) and reflectivity (B) in the electrode after different plasma treatment time.

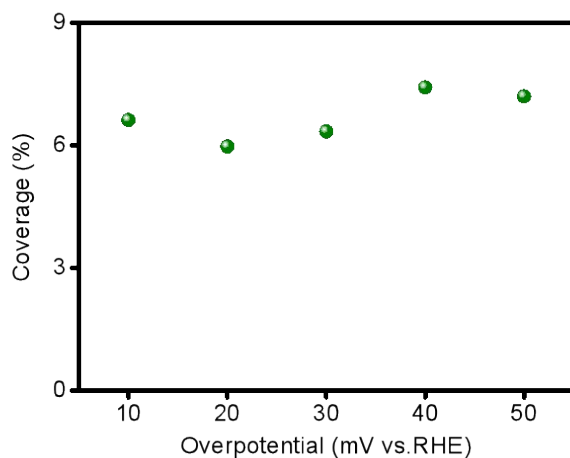


Fig. S18 Coverage of nanobubbles under different overpotentials.

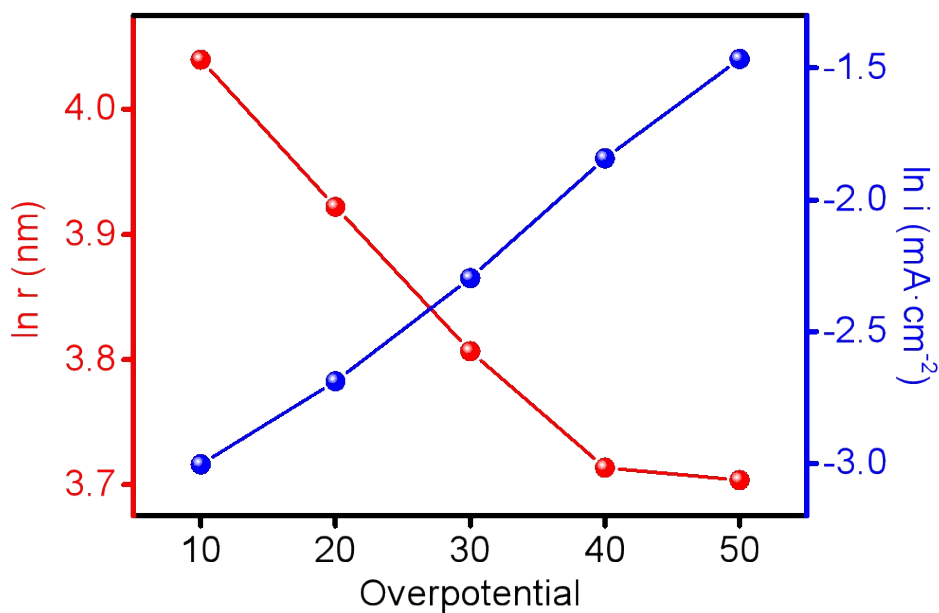


Fig. S19 Variation curve of $\ln(r)$ and $\ln(i)$ with overpotential.

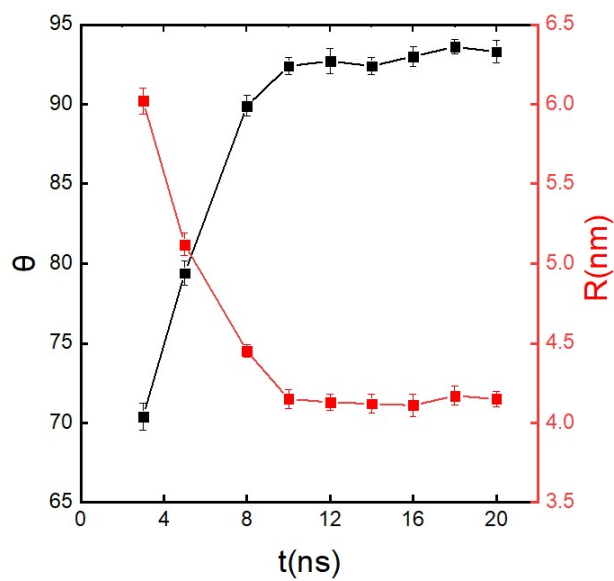


Fig. S20 The variation of contact angle and curvature radius of nanobubbles.

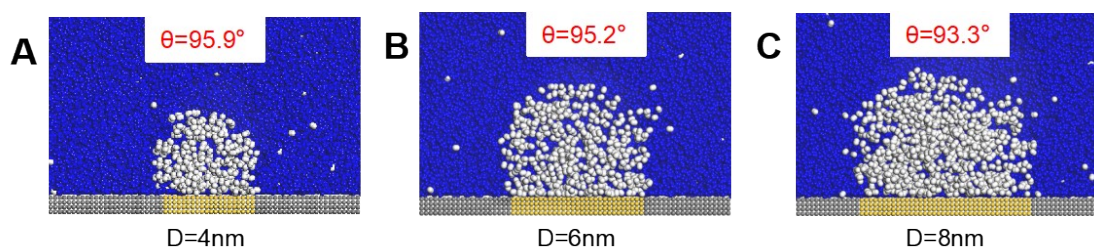


Fig. S21 Simulated contact angles of equilibrium nanobubble at different sized electrodes.

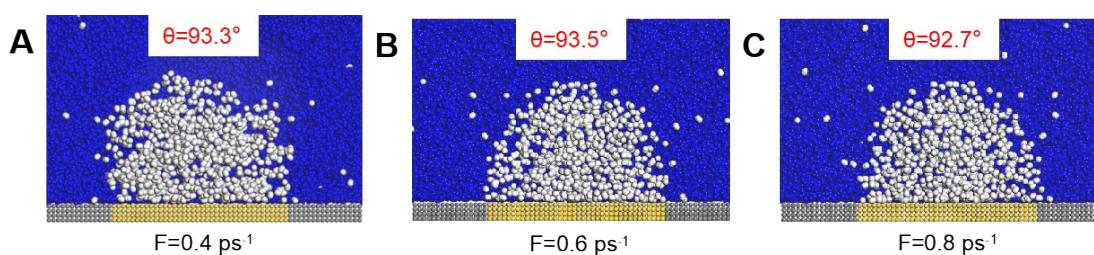


Fig. S22 Snapshots of nanobubbles with different driving force F .

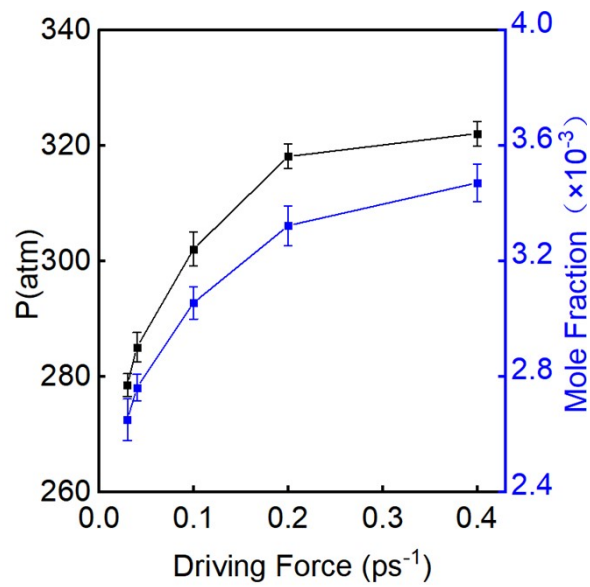


Fig. S23 Simulated variation of pressures of nanobubbles and the molar fractions with different driving forces.